

Omar M. Basha, Li Weng, Zhuo-wu Men, Wayne Xu, Badie I. Morsi

NICE's Indirect Coal-to-Liquid Process for Producing Clean Transportation Fuels Using Fischer-Tropsch Synthesis

Abstract China is currently the world's top coal consumer and the largest oil importer to sustain its rising economy and meet the mounting demand for transportation fuels. However, the increasing emissions due to the huge fossil fuels consumption, coupled with oil market instability, could derail China's economic growth and jeopardize its national energy security. To face such a hurdle, China has been aggressively supporting low-carbon businesses opportunities over the past decade, has recently announced several plans to cap coal utilization, and is currently the biggest investor in clean energy technologies. Coal-to-Liquid (CTL) is one of the most promising clean coal technologies, offering an ideal solution that can meet China's energy demands and environmental expectations. It is widely known that the Shenhua Group has pioneered and is currently leading the commercialization of the Direct Coal Liquefaction (DCL) process in China.

This paper highlights a part of the joint research effort undertaken by the National Institute of Clean-and-Low-Carbon Energy (NICE) and University of Pittsburgh in order to develop and commercialize the Indirect Coal Liquefaction (ICL) process. In this mission, NICE has built and operated an ICL plant including a large-scale (5.8-m ID and 30-m height) Slurry-Bubble-Column Reactor (SBCR) for Fischer-Tropsch synthesis using iron catalyst. The research, conducted at the University of Pittsburgh over the past few years, allowed building a user-friendly Simulator, based on a comprehensive SBCR model integrated with Aspen Plus and is validated using data from the NICE actual ICL plant. In this paper, the Simulator predictions of the performance of the NICE SBCR, operating with iron

and cobalt catalysts under four different tail gas recycle strategies: (1) direct recycle; (2) using a Pressure Swing Adsorption (PSA) unit; (3) using a reformer; and (4) using a Chemical looping Combustion (CLC) process, are presented. It should be mentioned also that our joint research effort has laid the foundation for the design of a commercial-scale SBCR for producing one-million tons per annum of environmentally friendly and ultraclean (no sulfur, no nitrogen and virtually no aromatics) transportation fuels, which could greatly contribute to ensuring China's national energy security while curbing its lingering emission problems.

Keywords: Fischer-Tropsch synthesis, tail gas recycle, simulations, process design

1 Introduction

Driven by a rapidly growing economy and a huge population, China's energy demand has nearly doubled since 2005. In 2009, China was the world's largest energy producer, and in 2010, it surpassed the U.S. and became the world's largest energy consumer. In 2011, China became the world's largest power generator, due to its sizable industrialization and emerging economy (Liu, 2015). In 2013, China consumed 25% more energy than the U.S., and it was estimated that by 2014 China will consume more than twice as much energy as the U.S. (U.S. Energy Information Administration, 2014). China is the world's top coal producer and consumer and its share is almost half of the global coal consumption (World Bank, 2014). In 2012, coal accounted for about 87% of China's total energy production (see *Figure 1(a)*) and represented nearly 66% of the total energy consumption, whereas oil accounted only for about 20% (see *Figure 1(b)*). China is also the world's largest importer of crude oil (British Petroleum, 2014) and in 2014, China's share of world's gross oil consumption was 43% (U.S. Energy Information Administration, 2014). China's coal-dominant energy mix, which would

Manuscript received February 29, 2016; accepted September 30, 2016

Omar M. Basha, Badie I. Morsi (✉)
Department of Chemical and Petroleum Engineering, University of Pittsburgh, Pittsburgh, PA 15261, USA
Email: morsi@pitt.edu

Li Weng, Zhuo-wu Men, Wayne Xu
National Institute of Clean-and-low-carbon Energy, Beijing 102209, PR China

not change in the near future, resulted in significant environmental concerns. In 2014, China was responsible for 25% of global carbon dioxide emission (see *Figure 2 (a)*), primarily due to the significant hike in coal consumption for electricity generation and cement production (Liu, 2015; World Bank, 2014), even though China's carbon dioxide emissions per capita were significantly lower than those in the U.S. and Russian Federation (*Figure 2 (b)*). Moreover, China's unprecedented industrialization and rising standards of living led to the increase of SO_x , NO_x and volatile organic compounds (VOC) emissions, which are the precursors of smog formation. Actually, in December 2015, dangerous smog levels up to 268 micrograms per cubic meter were reported in Beijing, forcing the Government to issue a red alert warning (Liu, 2015).

China has recognized that such significant environmental effects pose a threat to achieving the desired economic growth, and has subsequently started implementing a long term, multi-faceted plan targeting both industrial and vehicular emissions, with the goal of decreasing CO_2 , VOC, SO_x , and NO_x emissions to globally accepted levels (Liu, 2015). In addition, the increasing reliance of China on oil imports could also be another threat for achieving national security. In fact, China imports at least 51% of its oil from the unstable Middle East (British Petroleum, 2014) of which about 43% has to cross the Strait of Hormuz; and 82% of all Chinese maritime oil imports has to cross the Strait of Malacca (British Petroleum, 2014). The challenge is both straits are highly vulnerable to political conflicts, which could become a significant threat to China's energy security.

In order to face and overcome these threats, China has been developing alternative energy sources in order to achieve energy independence, without having a significant environmental footprint. More importantly, China has

recently announced plans to cap coal use to 62% of the total primary energy consumption by 2020, in an effort to reduce the air pollution which has afflicted certain areas of the country in recent years (Liu, 2015). China has increased its use of natural gas and oil as clean burning fossil fuels and is planning to use natural gas for 10% of its energy consumption by 2020. China has also set targets to increase the non-fossil fuel energy consumption to 15% of the total energy mix by 2020 and to 20% by 2030 in an effort to ease the country's dependence on coal (Liu, 2015). Moreover, China has shown significant support in expanding low carbon businesses opportunities (*Figure 3*), as new financial investments over the past decade have grown exponentially. As a matter of fact, China is currently the biggest investor in clean energy technologies, surpassing both the U.S. and EU, with particular interest in developing clean coal technologies (National Science Board, 2014).

Coal-to-Liquid (CTL) is one of the most promising clean coal technologies, which offers an ideal solution to China's energy demands and environmental expectations. In this process, coal is converted into liquid hydrocarbons, which are fed to existing refineries as a feedstock. Upon upgrading, the products can be utilized by the automobile and petrochemical industries without drastic changes to their operational landscapes. In addition, the CTL process yields clean transportation fuels, which ultimately reduce SO_x and NO_x emissions and enable the use of high efficiency engines, while providing an opportunity for CO_2 capture.

The purpose of this paper is to highlight some of the joint efforts undertaken by the National Institute of Clean-and-low-carbon Energy (NICE) and the University of Pittsburgh in order to control emissions by producing environmentally-friendly, ultraclean (sulfur- and nitrogen-free and virtually no aromatics) transportation fuels via the development of the indirect Coal-to-Liquid (ICL) process.

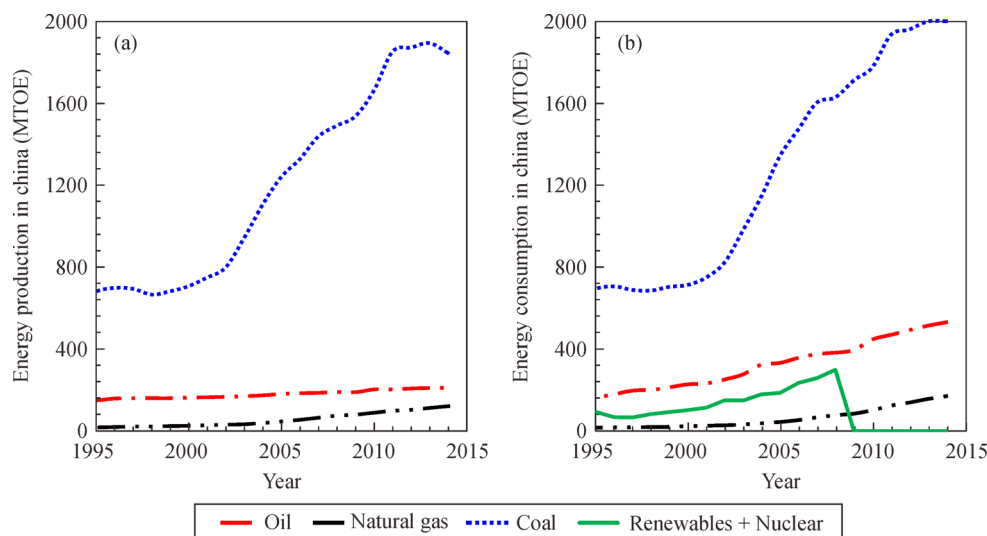


Figure 1. Fossil energy production (a) and consumption (b) in China (World Bank, 2014).

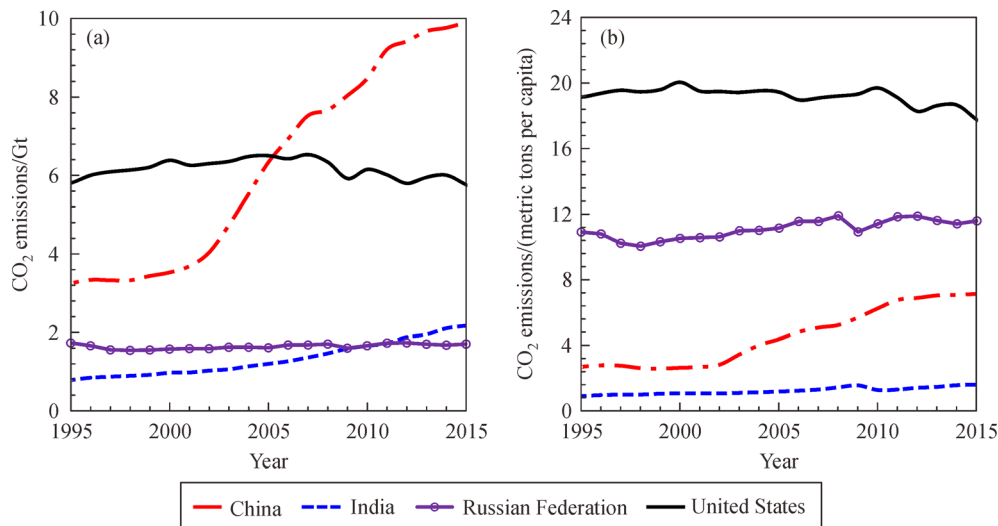


Figure 2. Total CO₂ emissions (a) and CO₂ emissions per capita (b) (World Bank, 2014).

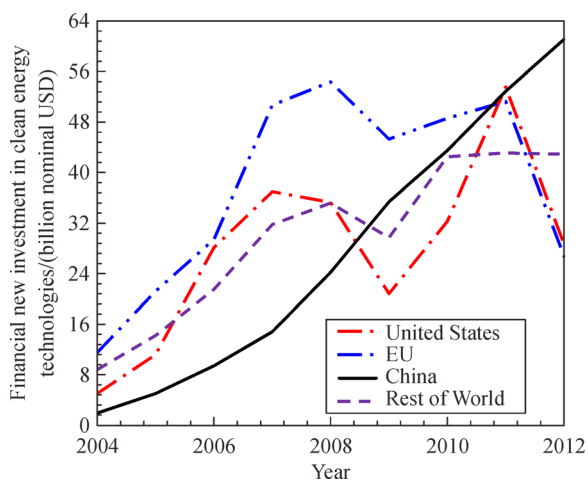


Figure 3. New investments in clean energy over the past decade (National Science Board, 2014).

Reactor modeling, optimization, and different strategies for tail gas recycle are presented.

2 Direct and indirect coal liquefaction

The CTL technologies include direct coal liquefaction (DCL) and indirect coal liquefaction (ICL) processes as shown in Figure 4. The DCL process encompasses pyrolysis, solvent extraction and catalytic extraction (Speight, 2012). Pyrolysis involves heating the coal to temperatures in excess of 400°C in order to convert it into gases, liquids and chars. Solvent extraction involves mixing the coal with a solvent (donor), capable of donating atomic or molecular hydrogen at temperatures up to 500°C and pressures up to 5000 psi, in order to dissolve or “break”

the coal into low molecular weight products. Catalytic liquefaction involves the use of a suitable catalyst, typically metal sulfides (e.g., FeS and FeS₂) or acid catalysts (e.g., FeCl₃ and ZnCl₂) in order to facilitate the injection of hydrogen into the coal matrix.

The ICL, on the other hand, is to react the coal with steam and oxygen (or air) in a gasifier to produce mainly a raw syngas (mixture of H₂ and CO). After removing of the particulates and sulfur-containing compounds, the clean syngas is shifted in a water-gas-shift (WGS) reactor to produce fuel gas containing more hydrogen and CO₂. The CO₂ is then removed and sent to sequestration sites, whereas the clean fuel gas is sent to an integrated gasification Combined Cycle (IGCC) for power generation. For fuels production, the H₂/CO ratio of the clean syngas stream is adjusted and subsequently used in a variety of processes, such as the Fischer-Tropsch (F-T) and methanol syntheses to produce clean transportation fuels.

It is widely known that The Shenhua Group has pioneered and is leading the commercialization of the DCL process in China. Therefore, this paper is focusing mainly on the joint effort by NICE and the University of Pittsburgh for the development of the ICL process using F-T synthesis.

3 Reactors for F-T synthesis

In the F-T synthesis, the syngas reacts in the presence of a heterogeneous catalyst to produce a wide range of hydrocarbon products, primarily linear alkanes and alkenes. Although many metals have been identified to catalyze the F-T reactions, only iron (FeO_x) and cobalt (Co) have been used beyond laboratory-scale applications (Basha, Sehabiague, Abdelwahab, & Morsi, 2015; Botes,

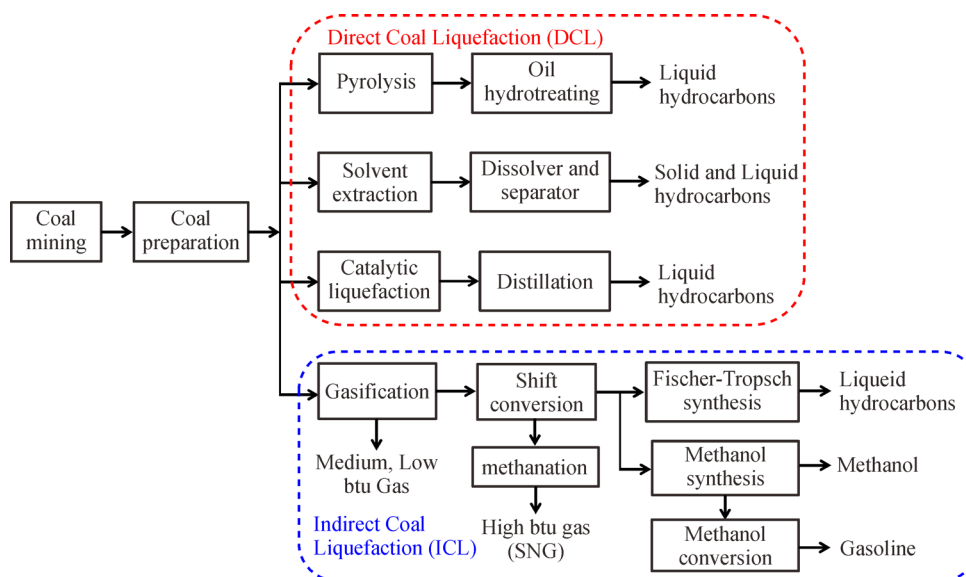


Figure 4. Schematic of the ICL and DCL processes.

Niemantsverdriet, & van de Loosdrecht, 2013; Wood, Nwaoha, & Towler, 2012). Depending on the reaction temperature, the F-T process is referred to as low-temperature F-T (LTFT) or high-temperature F-T (HTFT). The temperature of the LTFT ranges from 180°C to 260°C and produces heavy hydrocarbons (wax), which upon upgrading yield a variety of high-value products, such as middle distillates and naphtha. The temperature of the HTFT process is between 290°C and 360°C and the products are mostly gases and short chain hydrocarbons.

Figure 5 shows schematics of the different reactors used in high-temperature and low-temperature F-T processes. The HTFT process is conducted in fixed fluidized-bed reactors (FFBRs) and circulating fluidized-bed reactors (CFBRs), whereas the LTFT process is carried out in multi-tubular fixed-bed reactors (FBRs) and slurry-bubble-column reactors (SBCRs). In addition, a small-scale LTFT process can be carried out in micro-channel reactors (MCRs), even though no commercial MCRs are yet available.

The most recently used reactors for commercial F-T synthesis are FBRs and SBCRs. SBCRs were reported to have numerous advantages over FBRs (Dry, 2002; Steynberg, Dry, Davis, & Breman, 2004), including better temperature control and heat removal; lower capital cost, lower pressure drop, ability to use finer catalyst particles (< 100 µm), higher yield per reactor volume, and fewer necessary shutdowns as catalyst can be continuously added to or removed from the reactor. Despite these advantages, however, SBCRs inherit some drawbacks, such as strong liquid back-mixing, significant catalyst attrition, challenging catalyst separation from the heavy products, and complex hydrodynamics.

4 NICE contribution to China's clean coal technology

The National Institute of Clean-and-Low-Carbon Energy (NICE), a Research Institute in Beijing China, and a subsidiary of the Shenhua Group, considered the largest coal and energy producing company in the world, has undertaken the design and construction of an ICL plant employing a large-scale SBCR. The SBCR has 5.8-m ID and 30-m height, and operates with iron-based catalyst under pressures and temperatures up to 28 bar and 528 K, respectively.

The ongoing partnership between NICE and the University of Pittsburgh aims at modeling, optimization and ultimately scale up of the SBCR for the use in a commercial-scale F-T plant of one-million ton per annum capacity. The systematic research methodology devised at the University of Pittsburgh and applied to this joint project consists of the following main steps:

- (1) Develop a three-phase, two-dimensional transient reactor model (material, energy and momentum balances).
- (2) Identify and set the boundary and initial conditions.
- (3) Determine the unknown equation parameters.
- (4) Conduct an extensive literature search to seek these unknown parameters.
- (5) If the equation parameters are not available, measure them experimentally under actual F-T conditions in a pilot-scale SBCR (ID > 0.15-m) in order to eliminate the need for data corrections by pressure, temperature, reactor size, or system nature.
- (6) Solve the reactor model equations numerically and validate the model predictions against performance data taken from an actual F-T plant reactor.
- (7) Fine-tune the reactor model in order to predict the

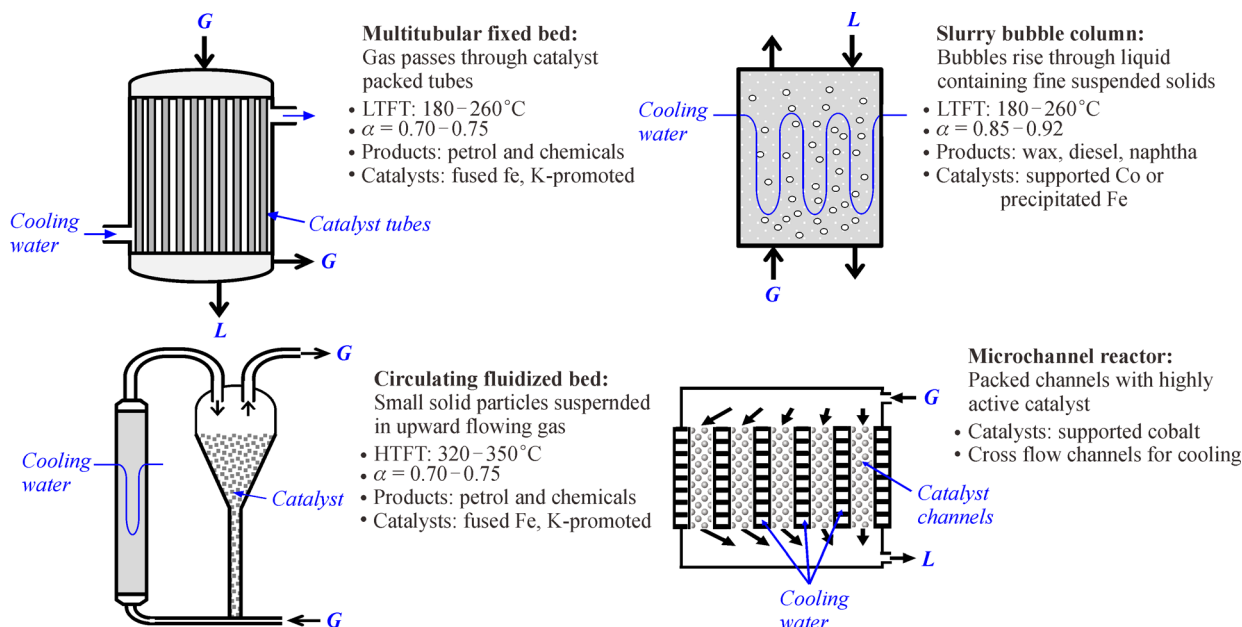


Figure 5. Reactors for F-T synthesis (Basha, Sehabiague, Abdelwahab, & Morsi, 2015).

actual F-T plant reactor performance with high accuracy.

(8) Integrate the reactor model with AspenPlus simulator for plant design and use it to optimize the performance of the F-T plant reactor using different strategies for tail gas recycle.

(9) Change the input and use the model for scale up the SBCR of the plant to the desired commercial-scale.

In our joint research effort, many equation parameters, including gas holdup (ϵ_G), Sauter-mean diameter of gas bubbles (d_{32}), and volumetric liquid-side mass transfer coefficients ($k_L a$), reaction kinetics were unknown in the model equations. The reaction kinetics for iron catalyst was provided by NICE. The extensive literature search, however, could not provide the other hydrodynamic and mass transfer parameters for syngas in F-T liquids under typical F-T conditions. Therefore, these parameters for He/ N_2 gaseous mixtures, as surrogates for H_2/CO , were measured in our pilot-scale SBCR (0.3 m ID, 3 m high), operating with an actual F-T reactor wax provided by NICE under typical synthesis conditions ($T = 380-550$ K, $P = 4-31$ bar, $u_g = 0.1-0.3$ m/s, $C_s = 0-45$ wt%). This pilot-scale SBCR, shown in Figure 6, is available at our Reactor and Process Engineering Laboratory (RAPEL), University of Pittsburgh and additional details can be found elsewhere (Sehabiague et al., 2015). The measured hydrodynamic and mass transfer parameters were then modeled incorporated into the reactor model for F-T SBCR developed by Sehabiague and Morsi (Sehabiague et al., 2008; Sehabiague & Morsi, 2013). The reactor model was implemented in our user-friendly Simulator, available at RAPEL, which was used to predict the syngas conversion, and C_1^+ as well as C_5^+ yields and the predictions were found to be in a very

good agreement with those of the actual NICE CTL plant.

Therefore, our Simulator was used to investigate the performance of the NICE CTL plant under different operating conditions, including catalyst concentration, reactor height/diameter ratio, reactor temperature/pressure, feed syngas flow rate and different catalyst/kinetics, etc. An example of such investigations is depicted in Figure 7 which shows the effects of catalyst concentration and reactor length-to-diameter ratio (L/D) on the water partial pressure, which is mainly responsible for the iron catalyst deactivation and affects the H_2 and CO conversions as well as the C_5^+ product yields (Sehabiague et al., 2015).

5 F-T process optimization using tail gas recycle

Our Simulator was further integrated with AspenPlus v8.6 using a customized unit operations model, which is a Fortran Subroutine of the Simulator. The Simulator was modified in order to accept as input the different stream variables from the AspenPlus simulation engine, and to deliver as output to AspenPlus the tail gas and liquid product flow rates and compositions with proper thermodynamic package.

The simulator was used to investigate the effects of direct tail gas recycle ratios on the syngas conversion, overhead hydrocarbons condensate (C_5^+) and wax yields using different kinetic rate expressions for Fischer-Tropsch (F-T) and Water-Gas-Shift (WGS) reactions. The simulations were conducted using NICE SBCR in the CTL plant using three kinetic expressions for iron catalyst, including one



Figure 6. Photographs of the SBCR (top) and gas distributor (bottom) at RAPEL.

provided by NICE, and three kinetic expressions for cobalt catalyst taken from the literature. The process with direct tail gas recycle used in this investigation is schematically shown in *Figure 8*.

In this process, the total syngas mixture (Stream 3) is heated (Stream 4) and enters NICE SBCR, where it is converted into hydrocarbon products. The liquid-phase products (molten wax) are recovered from the internal filter in the reactor (Stream 13), whereas the overhead products (vapor-phase) leave from the top of the reactor (Stream 5) to enter a vapor-liquid separator, where it is cooled to condense the hydrocarbons with carbon number, $C_n \geq 5$ as well as the reaction water (H_2O). The condensed

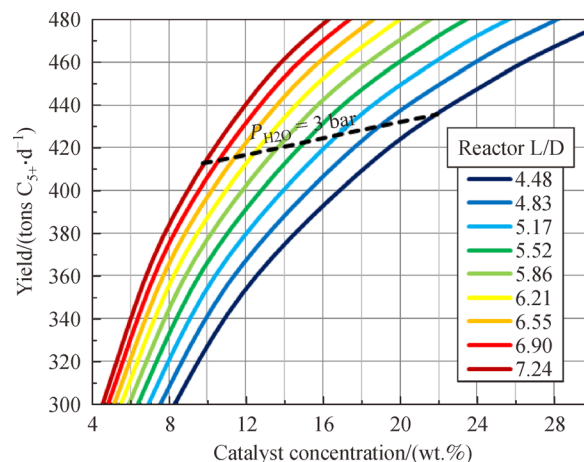


Figure 7. Effect of catalyst concentration and reactor height on C_5^+ products yield (Sehabiague et al., 2015).

hydrocarbons, called the overhead hydrocarbons condensate (C_5^+), are separated as (Stream 7) and the liquid water is separated as (Stream 6).

The vapor-phase exiting the top of the vapor-liquid separator (Stream 8) is called tail gas and it includes the unreacted syngas ($H_2 + CO$) as well as the light hydrocarbons with carbon number C_n , $C_n < 5$. A portion of this tail gas could be used for power generation or hydrogen production (Stream 9) and the balance (Stream 10) is compressed using compressor (2) to (Stream 11). A portion of this stream, which is taken at point B, is used to assist the removal of the wax from the reactor (Stream 14). The remaining balance (Stream 12) is recycled to mix at point A with the compressed fresh syngas feed (Stream 2) coming from compressor (1). The recycle ratio is defined as the ratio between the volumetric flow rate of the tail gas in (Stream 12) and the fresh syngas stream (Stream 2) coming from the main compressor (1).

Details of the NICE SBCR and operating variables used in the simulations are given in Table 1. The fresh syngas composition used (Stream 1) is given in Table 2. It should be emphasized that this fresh syngas contains no CO_2 and its sulfur content must be $< 0.02 \text{ mg/Nm}^3$ in order to avoid poisoning of the F-T catalyst (Dry, 2002). The F-T and WGS reaction kinetic rate expressions for the NICE iron catalyst are given in Table 3 and those for the other iron catalysts are shown in Table 4 and Table 5, respectively. In addition, those for the cobalt catalysts are provided in Table 6.

6 Direct tail gas recycle benchmarking

In order to benchmark the performance of incorporating a direct tail gas recycle strategy in the NICE plant, our simulations were conducted at different recycle ratios, ranging from 0 to 3 by volume. Four main metrics, (1) CO

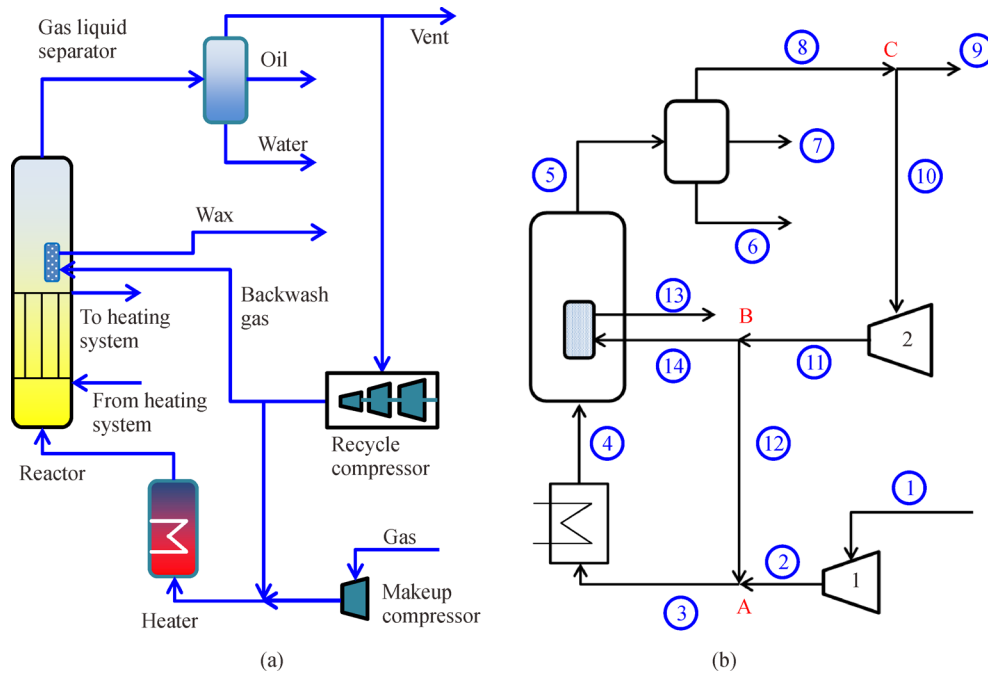


Figure 8. Process scheme with direct tail gas recycle (a), Stream numbers (b).

Table 1

NICE F-T SBCR Operating Conditions Used in the Simulations

Item	Parameter	Value
Reactor	L/m	30
	D/m	5.8
Sparger	Sparger coefficient/r	100
Cooling pipes	Number	604
	Outside diameter/m	0.057–0.089
Operating Variables	T/K	528
	P/bar	28
	$U_g/(m \cdot s^{-1})$	0.1–0.5
	Fresh syngas flow rate	125,000 Nm ³ /h (0°C and 1 atm)
	$U_L/(m \cdot s^{-1})$	0.00015
	Solid loading/kg	14,000

per-pass conversion, (2) H₂ per-pass conversion, (3) overhead hydrocarbons condensate (C₅⁺) yield, and (4)

Table 3

NICE Kinetics for Iron Catalyst Used in the Simulation

Catalyst	Reaction	T/°C	Equation	Parameters
NICE Catalyst (Fe)	F-T	255	$r_{FT} = \frac{k P_{CO} P_{H_2}}{P_{CO} + a P_{H_2O} + b P_{CO_2}}$	$k = 0.118 \text{ mol} \cdot \text{kg}^{-1} \cdot \text{s}^{-1} \cdot \text{MPa}^{-1}$ $a = 5.9$ $b = 5.9$
	WGS	255	$r_{CO_2} = \frac{k \left(P_{CO} P_{H_2O} - \frac{P_{H_2} P_{CO_2}}{K_p} \right)}{(P_{CO} + a P_{H_2O} + b P_{CO_2})^2}$	$k = 0.083 \text{ mol} \cdot \text{kg}^{-1} \cdot \text{s}^{-1}$ $a = 1.9$ $b = 1.9$ $K_p = 79.7$

Table 2

Fresh Syngas Composition Used in the Simulation

Component	Mole Fraction
H ₂	0.5247
CO	0.3446
CO ₂	0.0002
N ₂	0.1272
O ₂	0.0027
CH ₄	0.0003
H ₂ S	< 0.02 mg/Nm ³

wax yield, were obtained to evaluate the reactor performance.

Figure 9 (a) and (b) shows the effect of recycle ratio on the CO per-pass conversion for the three iron and three cobalt kinetic rate expressions used in the simulation, respectively. As can be seen in this figure, increasing the recycle ratio decreases the per-pass CO conversion for all

Table 4*Literature Kinetics of Iron Catalyst Used in the Simulation*

Catalyst	Operating Conditions	Equation	Reference
Fe/Cu/K/SiO ₂	Slurry Reactor T = 250°C–290°C P = 1.0–2.5 MPa H ₂ /CO _{feed} = 0.67–1.5	$r_{\text{CH}_4} = K_1 K_2 K_3 K_6 k_{7,M} K_4^{0.5} \frac{P_{\text{CO}} P_{\text{H}_2}^{2.5}}{P_{\text{H}_2\text{O}}} [S]^2$ $r_{\text{C}_n\text{H}_{2n+2}} = K_1 K_2 K_3 K_6 k_7 K_4 \frac{P_{\text{CO}} P_{\text{H}_2}^3}{P_{\text{H}_2\text{O}}} \prod_{i=2}^n \alpha_i [S]^2$ $+ P_{\text{H}_2} k_n \frac{k_8 - P_{\text{C}_n\text{H}_{2n}}^* [\sigma]}{k_n P_{\text{H}_2} + k_{8,+}}, (n \geq 2)$ $r_{\text{C}_n\text{H}_{2n}} = K_1 K_2 K_3 k_{8,+} (1 - \beta_n) \frac{P_{\text{CO}} P_{\text{H}_2}^2}{P_{\text{H}_2\text{O}}} \prod_{i=2}^n \alpha_i [S]^2$ $- P_{\text{H}_2} k_n \frac{k_8 - P_{\text{C}_n\text{H}_{2n}}^* [\sigma]}{k_n P_{\text{H}_2} + k_{8,+}}, (n \geq 2)$	Chang et al., 2007
Fe/Mn& Fe/Cu/K	Spinning Basket Reactor T = 260°C–300°C P = 1.1–2.6 MPa H ₂ /CO _{feed} = 0.67–2.05	$r_{\text{CH}_3\text{OH}} = k_{9,1} K_1 K_4 K_7 K_8 P_{\text{CO}} P_{\text{H}_2}^2 [S]^2$ $r_{\text{CH}_4} = k_{11,1} \alpha_{T,1} K_2 P_{\text{H}_2} [S]^2$ $r_{\text{C}_n\text{H}_{2n+1}\text{OH}} = k_9 K_1 K_4 K_7 K_8 P_{\text{CO}} P_{\text{H}_2}^2 \prod_{i=1}^{n-1} \alpha_{T,1} [S]^2$ $r_{\text{C}_n\text{H}_{2n-1}\text{OOH}} = \frac{k_{10} K_1 K_7 P_{\text{CO}} P_{\text{H}_2\text{O}}}{K_6} \prod_{i=1}^{n-1} \alpha_{T,1} [S]^2$ $r_{\text{C}_n\text{H}_{2n+2}} = k_{11} K_4 P_{\text{H}_2} [S]^2 \prod_{i=1}^n \alpha_{T,1}$ $r_{\text{C}_n\text{H}_{2n}} = k_{12} \sqrt{K_4 P_{\text{H}_2}} [S] \prod_{i=1}^n \alpha_{T,1} (1 - \beta_n)$	Teng et al., 2006

Table 5*Literature WGS Kinetics for Iron Catalyst Used in the Simulation*

Catalyst	Operating Conditions	Equation	Reference
Fe/Cu/K/SiO ₂	Slurry Reactor T = 250°C–290°C P = 1.0–2.5 MPa H ₂ /CO _{feed} = 0.67–1.5	$r_{\text{WGS}} = \frac{a \left(\frac{P_{\text{CO}} P_{\text{H}_2\text{O}}}{P_{\text{H}_2}^{0.5}} - \frac{P_{\text{H}_2}^{0.5} P_{\text{CO}_2}}{K_{\text{eq}}} \right)}{\left(1 + b \frac{P_{\text{CO}} P_{\text{H}_2\text{O}}}{P_{\text{H}_2}^{0.5}} \right)^2}$	Chang et al., 2007
Fe/Mn& Fe/Cu/K	Spinning Basket Reactor T = 260°C–300°C P = 1.1–2.6 MPa H ₂ /CO _{feed} = 0.67–2.05	$r_{\text{WGS}} = \frac{a \left(P_{\text{CO}} P_{\text{H}_2\text{O}} - \frac{P_{\text{H}_2} P_{\text{CO}_2}}{K_{\text{eq}}} \right)}{c P_{\text{H}_2}^{0.5} + P_{\text{H}_2} + d \frac{P_{\text{CO}} P_{\text{H}_2\text{O}}}{P_{\text{H}_2}}}$	Teng et al., 2006

the kinetic rate expressions used in the simulation. In addition, the NICE reaction kinetics exhibited the highest per-pass CO conversions when compared with those of the iron and cobalt kinetics used.

Similarly, *Figure 9 (c) and (d)* shows that increasing the recycle ratio decreases the per-pass H₂ conversion for all

the kinetic rate expressions used in the simulation. Moreover, the NICE reaction kinetics exhibited the highest per-pass H₂ conversion when compared with those of the different iron catalyst kinetics used. However, the cobalt reaction kinetics by Todici et al. (2013) and van Steen and Schulz (1999) show greater per-pass H₂ conversions than

Table 6*Literature Kinetics of Cobalt Catalyst Used in the Simulation*

Catalyst	Operating Conditions	Equation	Reference
Co-Re/Al ₂ O ₃	Batch Reactor T = 205°C, 220°C, 230°C P = 1.5, 2.5 MPa H ₂ /CO _{feed} = 1.4, 2.1	$r_{\text{CH}_4} = k_{SM} K_7^{0.5} P_{\text{H}_2}^{1.5} \alpha_1 [S]$ $r_{\text{C}_2\text{H}_4} = k_{6E,0} e^{2c} \sqrt{K_7 P_{\text{H}_2}} \alpha_1 \alpha_2 [S]$ $r_{\text{C}_n\text{H}_{2n+2}} = k_5 K_7^{0.5} P_{\text{H}_2}^{1.5} \alpha_1 \alpha_2 \prod_{i=3}^n \alpha_i [S] \quad n \geq 2$ $r_{\text{C}_n\text{H}_{2n}} = k_{6,0} e^{cn} \sqrt{K_7 P_{\text{H}_2}} \alpha_1 \alpha_2 \prod_{i=3}^n \alpha_i [S] \quad n \geq 3$ $[S] = 1 / \left\{ \begin{array}{l} 1 + \sqrt{K_7 P_{\text{H}_2}} \\ + \sqrt{K_7 P_{\text{H}_2}} \left(1 + \frac{1}{K_4} + \frac{1}{K_3 K_4 P_{\text{H}_2}} \right) \cdot \left(\alpha_1 + \alpha_1 \alpha_2 + \alpha_1 \alpha_2 \sum_{i=3}^n \prod_{j=3}^i \alpha_j \right) \end{array} \right\}$	Todic et al., 2013
Co/MgO/ThO ₂ /SiO ₂ & Co/SiO ₂	Slurry Reactor T = 190°C–210°C P _{H₂} = 0.01–1.93 MPa P _{CO} = 0.05–2.54 MPa	$r_{FT} = \frac{k_{FT} P_{\text{H}_2}^{1.5} P_{\text{CO}}}{P_{\text{H}_2\text{O}} \left(1 + a (P_{\text{H}_2} P_{\text{CO}_2} / P_{\text{H}_2\text{O}}) \right)^2}$	van Steen & Schulz, 1999
Co/MgO/SiO ₂	Slurry Reactor T = 220°C–240°C P = 1.5–3.5 MPa H ₂ /CO _{feed} = 1.5–3.5	$r_{FT} = \frac{k_{FT} P_{\text{H}_2} P_{\text{CO}}}{(1 + a P_{\text{CO}})^2}$	Yates & Satterfiel, 1991

that of the NICE iron reaction kinetics.

Figure 10(a) and (b) shows the effect of recycle ratio on the overhead hydrocarbon condensate (C₅⁺) yield for the three iron and three cobalt kinetic rate expressions used in the simulation respectively. As can be seen in Figure 10(a), the NICE kinetics give the highest overhead hydrocarbon condensate yield when compared with those of the two other iron kinetics used. Figure 10(b), however, shows that the cobalt reaction kinetics by Todici et al. (2013), followed by that by van Steen and Schulz (1999), result in significantly greater overhead condensate yields than that obtained using NICE iron reaction kinetics.

Similarly, Figure 10(c) and (d) show the effect of recycle ratio on the wax yield for the three iron and three cobalt kinetic rate expressions used in the simulation, respectively. As can be seen in Figure 10(c), the NICE kinetics give the highest wax yield when compared with those of the two other iron kinetics used. Figure 10(d), however, shows that the cobalt reaction kinetics of Todici et al. (2013), followed by that of van Steen and Schulz (1999), result in significantly greater wax yields than those obtained using NICE iron reaction kinetics.

7 Tail gas recycle strategies to enhance the performance of NICE reactor

Subsequent to benchmarking the direct tail gas recycle,

three different options, (1) Pressure Swing Adsorption (PSA) unit for separation and H₂ recycle; (2) Reformers to adjust the tail gas composition before recycling; and (3) Chemical Looping Combustion (CLC) process for tail gas processing and H₂ recycle, were investigated as potential strategies for improving the performance of the NICE reactor.

7.1 The use of PSA strategy

The separation of pure H₂ from the tail gas stream for use in the hydrogenation of F-T heavy products is accomplished through a PSA unit. In our simulation, a H₂ purity of 100% was assumed; and the separation efficiency and tail gas pressure were assumed to be 74% and 1.36 bar, respectively, similar to those of the base case by Papadias, Ahmed, Kumar, and Joseck (2009). Also, the tail gas stream was heated/cooled to 40°C before entering the PSA unit following the work by Grande (2012), who reported that the optimum absorption temperature for PSA is about 32°C–49°C.

The schematic flow diagram of using the PSA strategy is shown in Figure 11, and the simulation results for the performance metrics are summarized in Table 7. As can be observed in this table, the recycle ratio at the maximum overall products yield ranges from 0.27 to 0.35, for all the kinetic rate expressions used. It should be noted that the increase or decrease in the values listed in Table 7 is

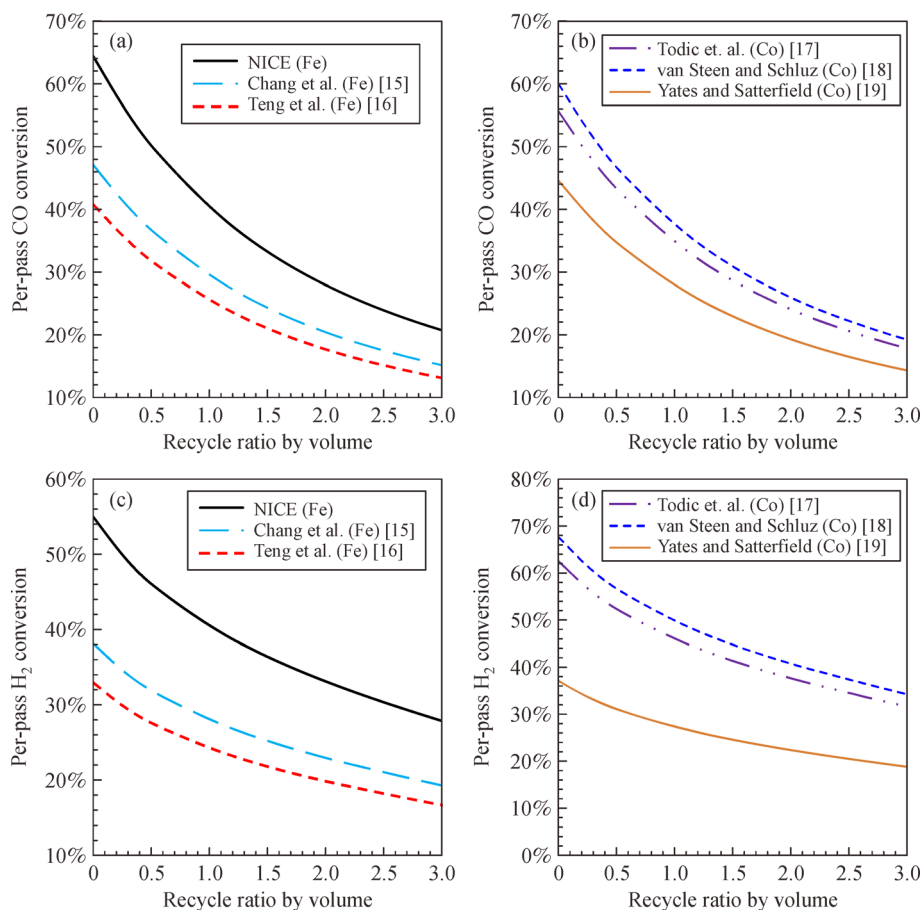


Figure 9. Effects of recycle ratio on CO per-pass conversion for (a) iron and (b) cobalt kinetics, and on H₂ per-pass conversion for (c) iron and (d) cobalt kinetics.

calculated with respect to the metrics of the benchmark, which is direct tail gas recycle, as described above. Moreover, for the six kinetic rate expressions used, this strategy appears to increase the overhead condensate yield by 4.15%–5.77% and the wax yield by 3.5%–5.6%.

7.2 The Use of reformer strategy

The organic components in the tail gas consist mainly of C₁–C₄ hydrocarbons and unreacted syngas (H₂ + CO) could be sent to a reformer. After their conversion, the produced syngas can be recycled to the F-T reactor. In addition, some of the CO₂ produced from the gasification plant or the WGS reactor could be used to reform the methane and other volatile hydrocarbons in the tail gas as:



If the Heat Recovery Steam Generation (HRSG) units in the gasification or power generation plants produce steam, exceeding the amount consumed by the other units in the respective plants, the excess steam could be used to reform the C₁–C₄ hydrocarbons in the tail gas as:



Due to the highly endothermic nature of the reforming reactions shown in Eqs. (1) and (2), heat is required. In order to provide heat, some of the O₂ from the ASU unit could be used to provide the required heat by partial combustion of the hydrocarbons:



This tail gas reforming strategy includes reactors wherein catalytic steam reforming (SR), or auto-thermal reforming (ATR) or partial oxidation (POX) of the light hydrocarbons into syngas takes place. Each one of these units is simulated using a Gibbs Reactor in AspenPlus. It is important to note that both ATR and POX require an expensive air separation unit (ASU) in order to produce the oxygen required for partial oxidation of the hydrocarbons. The ASU unit was modeled based on the assumptions made by Liu, Larson, Williams, Kreutz, & Guo (2011). Moreover, an O₂:C ratio of 0.6 was fixed in the input stream to the reformer (de Klerk, 2011) and the exit temperature of the reformer was maintained at 1000°C by

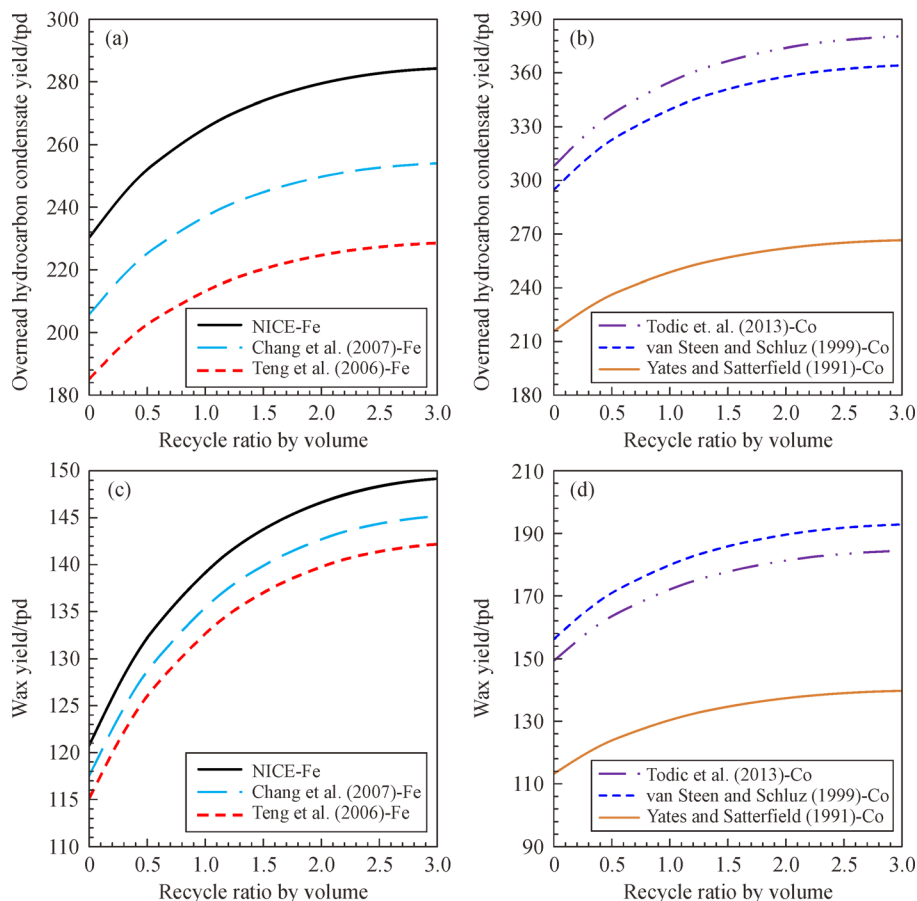


Figure 10. Effects of recycle ratio on the overhead hydrocarbon condensate yield for (a) iron and (b) cobalt kinetics; and on the wax yield for (c) iron and (d) cobalt kinetics.

Table 7

Performance Metrics for H_2 Recycle Using PSA Strategy

	Recycle ratio at maximum overall product yield	Maximum increase in overhead hydrocarbon condensate/%	Maximum increase in wax yield/%
NICE (Fe)	0.35	5.01	4.87
Chang (Fe) (Chang et al., 2007)	0.33	4.15	5.50
Teng (Fe) (Teng et al., 2006)	0.31	5.77	3.50
Todic (Co) (Todici et al., 2013)	0.27	4.25	4.95
van Steen and Schulz (Co) (van Steen & Schulz, 1999)	0.29	5.50	5.60
Yates and Satterfield (Co) (Yates & Satterfield, 1991)	0.28	5.20	4.25

adjusting the input steam flow rate.

A schematic diagram of this use of reformer strategy is shown in Figure 12 and the performance metrics for the different kinetic rate expressions used in our simulation are shown in Table 8. As can be observed in this table, the recycle ratio at the maximum overall product yield ranges from 1.29 to 1.63 for the six kinetic rate expressions used.

It should be noted that the increase or decrease in the values listed in Table 8 is calculated with respect to the metrics of the benchmark, which is direct tail gas recycle. In addition, for the six kinetic rate expressions used, this strategy appears to decrease the overhead condensate yields by 2.59%–4.34%, while increasing the wax yields by 2.13%–2.75%.

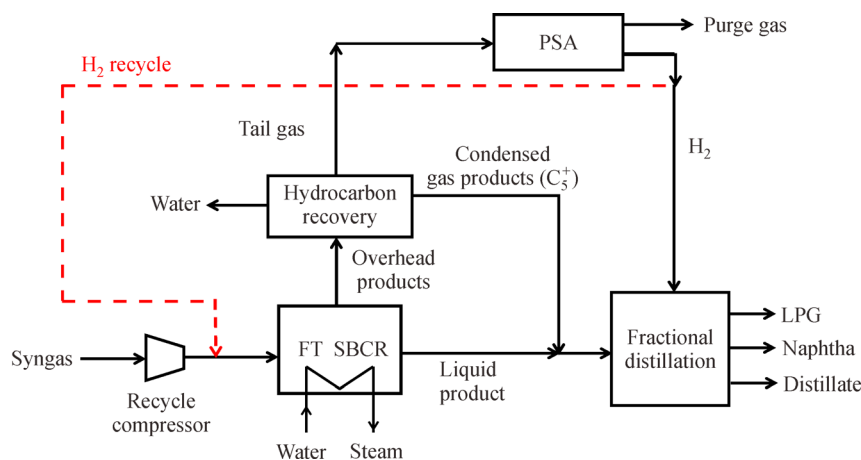


Figure 11. Schematic diagram of the use of PSA strategy.

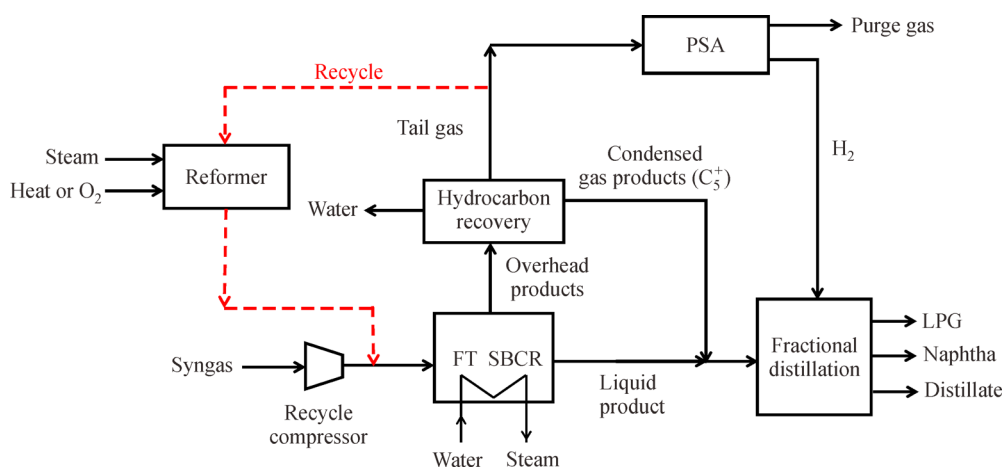


Figure 12. Schematic diagram of the use of reformer strategy.

7.3 The Use of chemical looping combustion strategy

The Chemical looping combustion (CLC) process was reported to provide a promising alternative for CO₂ capture from fuel gas streams by Fan (2010). In this strategy, the tail gas is first sent to a Fuel Reactor, where it reacts with iron oxides (Fe₂O₃) particles to produce CO₂ and H₂O and

consequently the iron oxide is reduced to Fe:

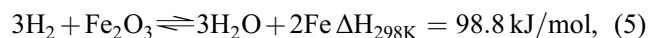
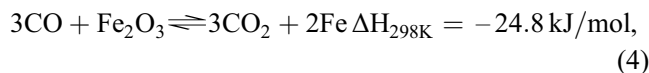
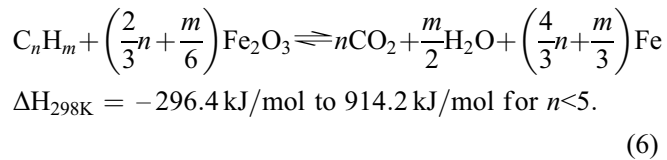


Table 8

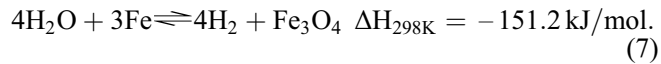
Performance Metrics for Tail Gas Reforming and Recycle Strategy

	Recycle ratio at maximum overall product yield	Maximum increase in overhead hydrocarbon condensate/%	Maximum increase in wax yield/%
NICE	1.47	-4.34	2.23
Chang (Fe) (Chang et al., 2007)	1.41	-3.40	2.13
Teng (Fe) (Teng et al., 2006)	1.43	-3.89	2.28
Todic (Co) (Todic et al., 2013)	1.32	-2.59	2.45
van Steen and Schulz (Co) (van Steen & Schulz, 1999)	1.40	-4.31	2.13
Yates and Satterfield (Co) (Yates & Satterfield, 1991)	1.63	-4.03	2.75

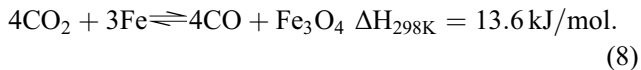


The reduced iron is then transferred to a Hydrogen Reactor.

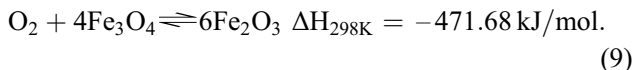
If steam (H_2O) is injected into the Hydrogen Reactor, it will react with the reduced Fe to produce H_2 as an output stream, while Fe is oxidized to Fe_3O_4 :



If CO_2 is also injected along with steam into the Hydrogen Reactor, CO_2 will react with the reduced Fe to produce CO, allowing the production of syngas as an output stream rather than only H_2 .



The iron oxide particles (Fe_3O_4) are then sent back to the Fuel Reactor using compressed air to be further oxidized to Fe_2O_3 :



The schematic diagram of this CLC strategy is shown in Figure 13, and the performance metrics corresponding to

the different kinetic rate expressions used are shown in Table 9. In this simulation, the conversions of the Fuel Reactor and the Hydrogen Reactor were assumed 100%. As can be observed in this Table, the recycle ratio at the maximum overall product yield ranges from 1.41 to 1.86 for all the kinetic rate expressions used.

Compared with the other two strategies, the use of CLC significantly increases the overhead condensate yield by 5.67%–8.4% and the wax yield by 5.88%–7.42%. Nonetheless, more investigations are needed in order to decrease the costs and enable commercialization of the CLC process. Once this is achieved, the CLC strategy would be useful, particularly, for processes, which emit huge volumes of CO_2 .

7.4 Effect of tail gas recycle strategies on CH_4 and CO_2 selectivities

Figure 14 shows the effect the four different tail gas recycle strategies on CO_2 and CH_4 selectivities as a function of the recycle tail gas ratio using NICE kinetics for iron catalyst (Table 3). The selectivity was defined as the number of moles of CO_2 or CH_4 in the overhead products stream, divided by the total number of the moles of the other species in this stream as given in Eq. (10). As can be seen in this figure, the selectivity of CH_4 increases with tail gas recycle ratio for the direct recycle strategy, but decreases for the other recycle strategies. In addition, the selectivity of CO_2 increases with tail gas recycle ratio for the reformer recycle strategy, but decreases for the other recycle

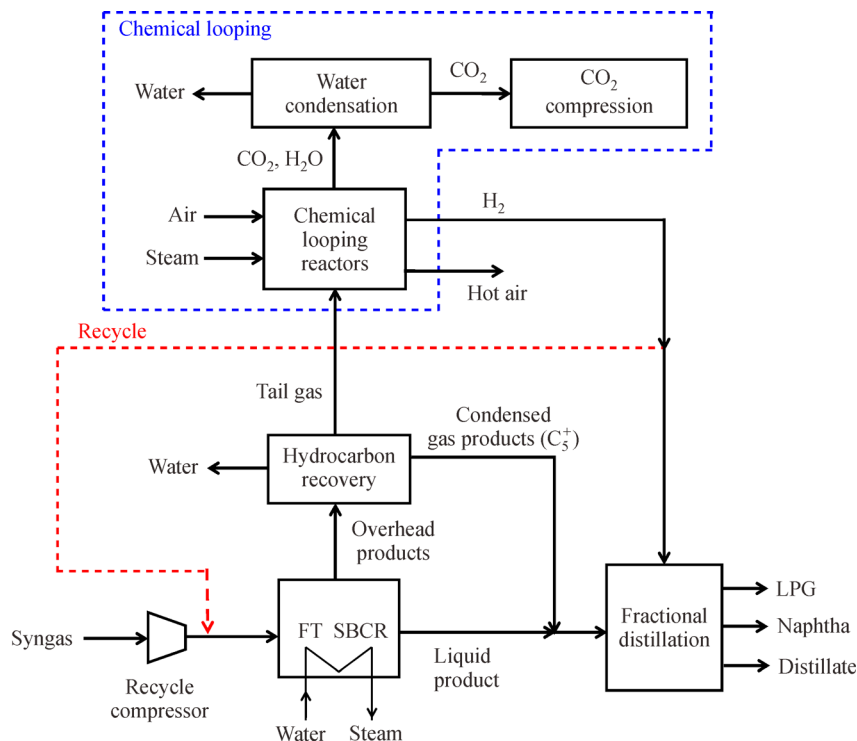


Figure 13. Schematic diagram of the use of CLC strategy.

Table 9*Performance Metrics for CLC Utilization Strategy*

	Recycle ratio at maximum overall product yield	Maximum increase in overhead hydrocarbon condensate/%	Maximum increase in wax yield/%
NICE (Fe)	1.41	5.67	6.51
Chang (Fe) (Chang et al., 2007)	1.56	7.35	5.88
Teng (Fe) (Teng et al., 2006)	1.67	7.63	6.37
Todic (Co) (Todic et al., 2013)	1.58	8.40	7.42
van Steen and Schulz (Co) (van Steen & Schulz, 1999)	1.79	8.26	6.93
Yates and Satterfield (Co) (Yates & Satterfield, 1991)	1.86	7.07	7.35

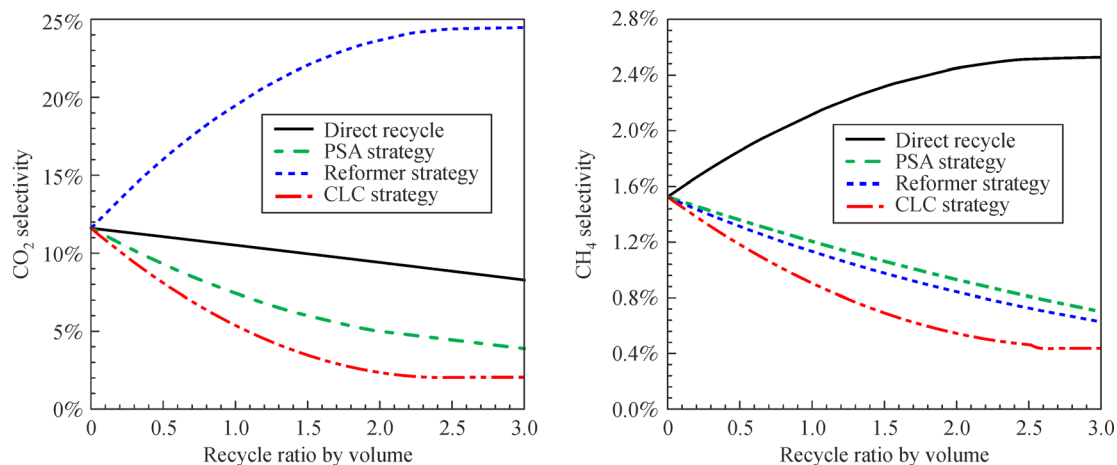


Figure 14. Effect of recycle ratio on the CO₂ selectivity (Left) and CH₄ selectivity (Right) for the different gas recycle strategies and NICE kinetics for iron catalyst.

strategies. It should be emphasized, however, the CLC recycle strategy decreases the CH₄ and CO₂ selectivities when increasing the tail gas recycle ratio.

$$Selectivity = \frac{n_{CO_2 \text{ or } CH_4}}{1 - n_{CO_2 \text{ or } CH_4}} \quad (10)$$

8 Concluding remarks

The research conducted at the University of Pittsburgh over the past few years allowed building a user-friendly Simulator, based on a comprehensive SBCR model integrated with AspenPlus and is validated using data from the NICE actual ICL plant, including a large-scale SBCR (5.8-m ID and 30-m height) for F-T synthesis using iron catalyst. The Simulator was used to investigate the effects of catalyst concentration and reactor length-to-diameter ratio (L/D) on the water partial pressure, which is mainly responsible for the iron catalyst deactivation and affects the H₂ and CO conversions as well as the C₅⁺ product yields in the NICE SBCR.

The Simulator was also used to predict the performance of the NICE SBCR, operating with three iron and three

cobalt catalyst kinetic rate expressions under four different tail gas recycle strategies: (1) direct recycle as a benchmark; (2) using a Pressure Swing Adsorption (PSA) unit; (3) using a reformer; and (4) using a Chemical looping Combustion (CLC) process. The Simulator predictions indicated that direct tail gas recycle decreased the per-pass conversions for H₂ and CO and significantly increased the overhead condensate and wax yields; and the use of a PSA unit for H₂ recycle increased the overhead condensate yield by 4.15%–5.77% and the wax yield by 3.5%–5.6%. Similarly, the use of CLC process increased the overhead condensate yield by 5.67%–8.4% and the wax yield by 5.88%–7.42%. However, the use of a reformer decreased the overhead condensate yield by 2.59%–4.34%, while increasing the wax yield by 2.13%–2.75%.

Thus, the use of tail gas recycle enhanced the SBCR performance for all the strategies investigated, except when using a reformer, with the CLC strategy showing the highest increase in the overhead hydrocarbon condensate and wax yields. In addition, the CLC strategy decreased the CO₂ and CH₄ selectivities when increasing the tail gas recycle ratio. Future work will focus on investigating the economic feasibility of implementing each of these recycle strategies, and on the prospect of integrating the CLC

technology with the coal gasification and Fischer-Tropsch processes.

Acknowledgements The Authors would like to thank the National Institute of Clean-and-Low-Carbon Energy (NICE), China, for their financial support of this research.

References

- Basha, O.M., Sehabiague, L., Abdelwahab, A., & Morsi, B.I. (2015). Fischer-Tropsch synthesis in slurry bubble column reactors: Experimental investigations and modeling—a review. *International Journal of Chemical Reactor Engineering*, 13, 201–288. Available at: <http://www.degruyter.com/view/j/ijcre.2015.13.issue-3/ijcre-2014-0146/ijcre-2014-0146.xml>.
- Botes, F.G., Niemantsverdriet, J.W., & van de Loosdrecht, J. (2013). A comparison of cobalt and iron based slurry phase Fischer-Tropsch synthesis. *Catalysis Today*, 215, 112–120. Available at: <http://www.doc88.com/p-7939538516115.html>.
- British Petroleum. (2014). *BP statistical review of world energy*. Retrieved from http://www.bp.com/content/dam/bp-country/de_de/PDFs/brochures/BP-statistical-review-of-world-energy-2014-full-report.pdf
- Chang, J., Bai, L., Teng, B., Zhang, R., Yang, J., Xu, Y., Xiang, H.W., & Li, Y.W. (2007). Kinetic modeling of Fischer-Tropsch synthesis over Fe-Cu-K-SiO₂ catalyst in slurry phase reactor. *Chemical Engineering Science*, 62, 4983–4991.
- de Klerk, A. (2011). *Fischer-Tropsch refining*. Retrieved from <http://onlinelibrary.wiley.com/book/10.1002/9783527635603>
- Dry, M.E. (2002). The Fischer-Tropsch process: 1950–2000. *Catalysis Today*, 71, 227–241.
- Fan, L.S. (2010). *Chemical looping systems for fossil energy conversions*. New York: John Wiley & Sons, Inc.
- Grande, C.A. (2012). *Advances in pressure swing adsorption for gas separation*. ISRN Chemical Engineering.
- Liu, G., Larson, E.D., Williams, R.H., Kreutz, T.G., & Guo, X. (2011). Making Fischer-Tropsch fuels and electricity from coal and biomass: performance and cost analysis. *Energy & Fuels*, 25, 415–437.
- Liu, Z. (2015). *China's carbon emissions report 2015*. Cambridge: Harvard Kennedy School of Government.
- National Science Board. (2014). *Science & engineering indicators*. Retrieved from <http://www.nsf.gov/statistics/seind14/>
- Papadakis, D.D., Ahmed, S., Kumar, R., & Joseck, F. (2009). Hydrogen quality for fuel cell vehicles—a modeling study of the sensitivity of impurity content in hydrogen to the process variables in the SMR-PSA pathway. *International Journal of Hydrogen Energy*, 34, 6021–6035.
- Sehabiague, L., Basha, O.M., Hong, Y., Morsi, B., Shi, Z., Jia, H., Weng, L., Men, Z., Liu, K., & Cheng, Y. (2015). Assessing the performance of an industrial SBCR for Fischer-Tropsch synthesis: experimental and modeling. *AIChE Journal. American Institute of Chemical Engineers*, 61, 3838–3857.
- Sehabiague, L., Lemoine, R., Behkish, A., Heintz, Y.J., Sanoja, M., Oukaci, R., & Morsi, B.I. (2008). Modeling and optimization of a large-scale slurry bubble column reactor for producing 10,000 bbl/day of Fischer-Tropsch liquid hydrocarbons. *Journal of the Chinese Institute of Chemical Engineers*, 39, 169–179.
- Sehabiague, L., & Morsi, B.I. (2013). Modeling and simulation of a Fischer-Tropsch slurry bubble column reactor using different kinetic rate expressions for iron and cobalt catalysts. *International Journal of Chemical Reactor Engineering*, 11, 1–22.
- Speight, J.G. (2012). *The chemistry a technology of coal*. USA: CRC Press
- Steynberg, P., Dry, M.E., Davis, B.H., & Breman, B.B. (2004). Fischer-Tropsch reactors studies. In A. Steynberg, B.V. Elsevier, & M. Dry (Eds.), *Studies in Surface Science and Catalysis*. Retrieved from <http://www.sciencedirect.com/science/bookseries/01672991/175>
- Teng, B., Chang, J., Zhang, C., Cao, D., Yang, J., Liu, Y., Guo, X., Xiang, H., & Li, Y. (2006). A comprehensive kinetics model of Fischer-Tropsch synthesis over an industrial Fe-Mn catalyst. *Applied Catalysis A, General*, 301, 39–50.
- Todic, B., Bhatelia, T., Froment, G.F., Ma, W., Jacobs, G., Davis, B.H., & Bukur, D.B. (2013). Kinetic model of Fischer-Tropsch synthesis in a slurry reactor on Co-Re/Al₂O₃ catalyst. *Industrial & Engineering Chemistry Research*, 52, 669–679.
- U. S. Energy Information Administration. (2014). *Annual energy outlook 2014*. Washington DC: Energy Information Administration.
- van Steen, E., & Schulz, H. (1999). Polymerisation kinetics of the Fischer-Tropsch CO hydrogenation using iron and cobalt based catalysts. *Applied Catalysis A, General*, 186, 309–320.
- Wood, D.A., Nwaoha, C., & Towler, B.F. (2012). Gas-to-liquids (GTL): a review of an industry offering several routes for monetizing natural gas. *Journal of Natural Gas Science and Engineering*, 9, 196–208. Available at: <http://www.sciencedirect.com/science/article/pii/S1875510012000947>.
- World Bank. (2014). *World development indicators*. Washington, DC: World Bank.
- Yates, I.C., & Satterfield, C.N. (1991). Intrinsic kinetics of the Fischer-Tropsch synthesis on a cobalt catalyst. *Energy & Fuels*, 5, 168–173.